Riveting Structure Modeling Based On Finite Element Method

Zhifang Lu[1] and Lin Yang[2*]

[1] School of Mechanical and Electrical Engineering, Hubei Science and Technology College, Wuhan 430074, China
[2] Department of Smelting, WISDRI Wuhan Iron and Steel Design and Research Institute Incorporation Limited, Wuhan 430083, China
[*] Corresponding author. E-mail: yanglinamtf@163.com

Received: January 22, 2024; Accepted: April 09, 2024

As an important technology in the field of machine manufacturing, metal riveting has been widely used in industrial manufacturing. However, in industrial production, the riveted structure is sometimes unstable, deformation, falling off and other dangerous situations, resulting in the failure of the riveted structure, which seriously endanger the life safety of employees. In this study, the riveted structure is modeled and failure analyzed by finite element analysis, and the deformation prediction model is constructed by finite element analysis of local elements of riveted structure. Firstly, the study conducts a small element modeling of riveted structures using finite element analysis methods, and conducts failure analysis of riveted structures based on multi angle rivet load displacement experiments. Afterwards, the layered mapping equivalent model is used to predict the deformation of the riveted structure after local element analysis, and the effectiveness of the prediction model is verified through finite element simulation. The study conducts relevant cases, and the results shows that the total error of the failure displacement of the riveted structure model is basically less than 10%, and the overall simulation results are good; The average stress of the riveting deformation prediction model is 490 MPa, and the detection effect is good. Therefore, the riveting structure model and deformation prediction model constructed in the study have good performance, which helps workers to timely handle risk factors and improve the safety of mechanical manufacturing.

Keywords: Rivet; Riveted structure; Stress; Plastic deformation; Finite element

http://dx.doi.org/10.6180/jase.202503_28(3).0017

1. Introduction

Currently, the manufacturing industry in industrial production is developing rapidly, and metal riveting is one of the important ways of connecting machine components, which is more widely used in the production of industrial machines [1]. The riveted structure is easy to disassemble and can be used to connect large steel components [2]. Generally, metal riveting is applied to the bearing part of the key parts of the machine, but it is also easy for the metal riveted structure to be torn by huge tension or shear [3]. Sometimes, due to the accumulated stress factors, the connection is partially broken, resulting in the failure of large machinery and even structural dislocation. In large transportation vehicles such as aircraft and ships, the failure and deformation of micro-riveted structure can threaten the life safety of all passengers. Therefore, it is very essential to model and analyze the metal riveted structure [4]. The previous modeling methods often rely too much on the experience of engineers and lack scientific and systematic analysis methods, which limits the prediction accuracy and application range of complex riveted structures to a certain extent. Therefore, the development of more accurate and comprehensive riveting structure modeling and prediction methods is of great significance for improving the riveting quality and ensuring the safety and stability of mechanical equipment [5, 6]. Therefore, it is indispensable to study the

deformation prediction of riveting results. In view of this, the riveted structure is modeled by small units through finite element analysis method, and the failure analysis of riveted structure is carried out according to the multi-angle rivet load displacement case. Meanwhile, the layered mapping equivalent model is used to predict the deformation of rivet structure after local unit analysis, and the effect of the prediction model is verified by finite element simulation, hoping to provide help for the progress of metal riveting technology. This study is divided into 5 parts: (1) The first part is the introduction, which mainly introduces the research background, research objectives, and the research status of the proposed technology. (2) The second part is the research method of the article, which mainly designs the riveting structure model and deformation prediction model. (3) The third part is case verification, mainly using ABAQUS 2021 software to test the performance of the riveting structure model and deformation prediction model. (4) The fourth part is the discussion section of the article, which mainly discusses the experimental results of this study. (5) The fifth part is the conclusion of this article, which mainly summarizes and prospects the content of the entire article.

Finite element analysis is a method of simulating real physical systems through mathematical approximation, which uses a set of simple and interrelated components to approximate a real system with infinite unknowns with a finite number of unknowns. This method can simplify complex problems, so it is widely popular among scientists. The finite element modeling of riveted structure is a common connection method for steel components, which has been discussed by many scholars. Figueira and Trabasso [7] conducted in-depth research on the extrusion force parameters in the riveting process of the aviation industry, and constructed a finite element model equation for checking the rivet head size based on the rivet material parameters. This equation could estimate the extrusion force at high extrusion ratios with small errors, compensating for the shortcomings of the original equation in ignoring the thickness of the riveting fixture and the friction force between the rivet, rivet plate, and punch. In response to the problem that the riveting process may cause deformation of parts in the aviation industry, Zanatta et al. [8] and his team proposed a riveting device model based on finite element analysis. The aim of this study was to find a scheme for determining induced deformation that could be applied to aircraft production lines from an industrial perspective. This scheme made full use of adaptive meshing to improve the overall accuracy of the model. This scheme fully utilized adaptive grids to improve the overall accuracy of the model. The case showed that this method had certain advantages. However, although adaptive mesh partitioning improved the accuracy of the model, it was still limited by the complexity and uncertainty of actual working conditions. Zamani and Farhangdoost [9] used finite element method to simulate the residual stress field and fatigue life of a single riveted tower joint. They took into account important riveting process parameters such as riveting force, sheet thickness, friction coefficient and clearance fit and optimized them to maximize the residual stress field. This study fully demonstrated the critical role of finite element modeling in predicting and optimizing the riveting process, but also revealed its limitations. Although the case results indicated good consistency between the model and actual observation data, it depended on the accuracy of the parameters and the complexity of the model.

Ji et al. [10] established a riveting model using the Ansoft Maxwell finite element analysis method to study the voltage load and stress conditions of riveted coils. By comparing simulation and experimental results, the tool structure was adjusted and the optimal riveting voltage range for stainless steel rivets was determined, thereby achieving good rivet head formation and interference fit between rivets and riveting plates. Wu and Chen [11] explored a lightweight design method using magnesium and aluminum alloys based on riveted structures. Through the repeated use of finite element simulation to calculate and verify the strength and mode, a design scheme with higher structural reliability was finally realized. This study demonstrated the critical role of finite element modeling in optimizing design and verifying structural strength. To create a simplified finite element model suitable for the riveted structure of a steel-aluminum hybrid car body, Song et al. [12] constructed a simplified model of double-row single-lap riveting and double-row double-lap riveting using the ANSYS platform and compared it with a full-solid model. It was found that this method, combined with sub model technology, could improve the computational efficiency of strength analysis of large riveted structures while ensuring accuracy.

In summary, although finite element modeling plays a significant role in the prediction and optimization of riveted structure, it has some limitations. The accuracy of the finite element model is limited by the accuracy of the input parameters. If the input parameters are wrong, the prediction may be biased. Secondly, the complexity of the model may make it less accurate in simulating the riveting process, leading to inaccurate predictions. Therefore, this study aims to solve the problem of metal riveted structures being prone to fracture under tensile or shear forces. Finite ele-

ment analysis is used to finely model the riveted structure, and combined with rivet load displacement experiments, the failure mode is analyzed in depth to improve the accuracy of model prediction. Compared to existing literature, this study adopts a new method combining multi angle experimental verification and layered mapping equivalent model, aiming to overcome the limitations of traditional empirical modeling methods in predicting the accuracy and application range of complex riveted structures, and thereby improve the design quality and safety of riveted structures.

2. Metal riveted structure modeling and deformation prediction

2.1. Riveting structure model design

To construct a metal riveted structure model, it is necessary to select a suitable modeling method. Since the damage increment model takes stress effect and nonlinear damage into consideration, it has high simulation accuracy . Among them, the nonlinear damage model can accurately reflect the nonlinear characteristics of material damage accumulation during the loading process. This model comprehensively considers the influence of stress state evolution on damage growth and can depict the stress-strain relationship throughout the entire process from micro damage initiation to macro failure. In riveted structures, local stress concentration and complex three-dimensional stress states lead to significant nonlinear characteristics in damage behavior. Thus, the use of nonlinear damage models is applicable for predicting material failure points and simulating the entire failure process. Therefore, a generalized damage increment model with measurable stress is adopted as the failure model for riveted structures. In the simulation of metal riveting structures, when the focus is on the macroscopic stress-strain relationship and overall structural behavior, it is often not necessary to consider the influence of mesh size. The main reason is that it is assumed that the notch test data is sufficient to characterize the plastic failure behavior of the material, without the need to capture detailed geometric details at the micro-scale. This assumption simplifies the simulation process and can improve computational efficiency without sacrificing the accuracy of critical structural responses. Without considering the influence of mesh size, the triaxial curve of plastic failure strain stress is fitted according to notch test data [13]. The bi-linear model of peak load failure is the material constitutive model of riveted joint structure, which can be used to establish beam element and solid element to simulate the failure of riveted structure. The riveted structure model can be divided into multiple solid analysis units by finite element analysis software, including hexahedron, 4-hexahedron cluster and 8-hexahedron cluster, as shown in Figure 1. The reasons for choosing "hexahedron, 4-hexahedron cluster and 8-hexahedron cluster" as solid analysis units are mainly based on their geometric properties and computational efficiency. Hexahedral elements are convenient for grid division due to their geometric shape rules, and have high adaptability when dealing with complex geometric structures [14]. The 4-hexahedral and 8-clusters of hexahedrons provide finer meshing for capturing local stress concentrations and failure areas. In addition, compared with other types of elements (such as tetrahedral elements), such elements have higher accuracy and higher computational efficiency in solving large deformation and nonlinear problems. Therefore, these elements are widely used in complex finite element analysis, including failure simulation of riveted structures.

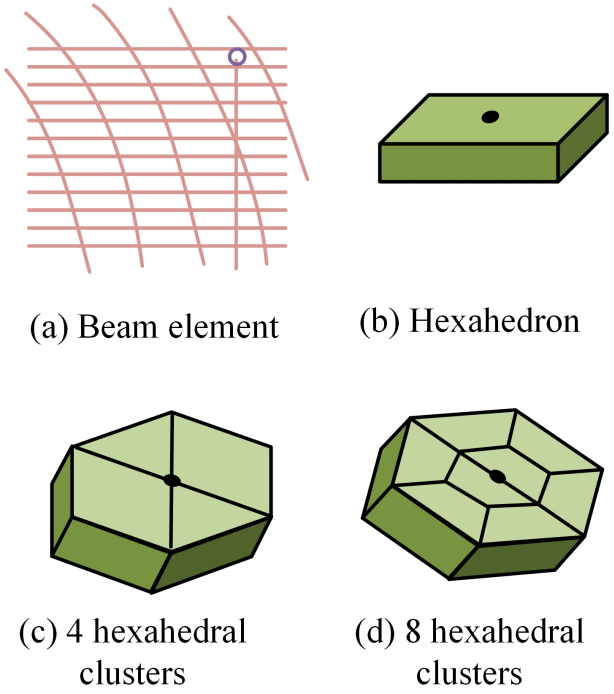

Fig. 1. Finite element analysis model.

Multiple hexahedra are combined with each other to form hexahedral cluster units, which are generally used to transfer stress and load. When the load of the hexahedron cluster element reaches the upper limit, the riveted structure will fail and the hexahedron cluster element will be deleted. The adoption of peak load failure criteria is based on the need for simplified analysis, which can focus on the behavior of riveted structures under maximum load. This criterion assumes that failure is mainly driven by normal

stress, while ignoring the effects of bending moment and torque on failure. This assumption allows for the neglect of complex stress states, simplifying failure analysis, accelerating the calculation process, and achieving moderate accuracy in estimating structural bearing capacity. Therefore, this study adopts the peak load failure criterion and ignores the influence of bending moment and torque on failure. The failure criterion for riveted structures is shown in Eq. (1).

$$P_{\text{fail}} = \sigma_{ut} \cdot A_{\text{rivet}} \tag{1}$$

In Equation (1), P_{fal} represents the peak load of the riveted structure when it reaches the failure state; σ_{ut} represents the ultimate tensile stress of the rivet material; A_{tivet} represents the cross-sectional area of the rivet. The failure criterion is shown in Eq. (2) [15].

$$\left(\frac{Nrr}{NRR}\right)^2 + \left(\frac{Nrs}{NRS}\right)^2 + \left(\frac{Nrt}{NRT}\right)^2 \leq 1 \tag{2}$$

In Eq. (2), Nrr refers to the tensile load on the riveted structural unit; Nrs and Nrt represent the shear component of the unit in directions s and t, respectively; NRR is the maximum tensile component of the riveted structural element; NRS and NRT are the maximum shear components of the unit in directions s and t, respectively. The schematic diagram of shear force components in different directions of riveted structural units is shown in Fig. 2.

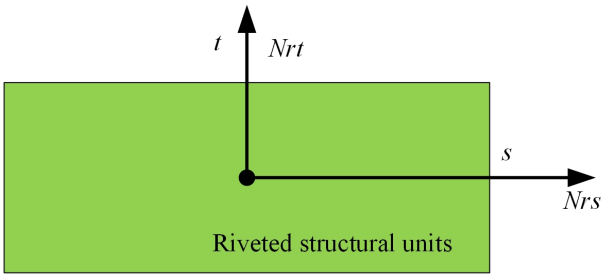

Fig. 2. Schematic diagram of shear force components in different directions of riveted structural units.

Using the force-based point connection constraint unit, the load displacement curve of the connected structure is formulated, as shown in Eq. (3) [16].

$$\eta_{\max} = \frac{\delta_n^{\max}}{\delta_n^{fail}} = \frac{\delta_t^{\max}}{\delta_t^{fail}} \tag{3}$$

In Eq. (3), $\eta_{\max}$ refers to the maximum load point of the model; $\delta_n^{\max}$ refers to the rivet displacement of the model under maximum load under shear; δ_n^{fail} is small displacement when the model is pure shear; $\delta_t^{\max}$ refers to the rivet displacement of the model under maximum load under tensile conditions; δ_t^{fail} refers to the failure displacement when the model is purely stretched. To adjust the shape of the model in the elastoplastic stage and determine the failure parameters of the riveted structure under different loading angles, the calculation process of the damage parameters of the model was defined as shown in Eq. (4) [17].

$$\alpha = \begin{cases} \frac{\xi_t - \eta_{\max}}{\xi_t}\alpha_1 + \frac{\eta_{\max}}{\xi_t}\alpha_2\eta_{\max} < \xi_t \\ \frac{1-\eta_{\max}}{1-\xi_t}\alpha_2 + \frac{\eta_{\max}-\xi_t}{1-\xi_t}\alpha_3\eta_{\max} \geq \xi_t \end{cases} \tag{4}$$

In Eq. (4), α refers to damage parameters; ξ_t refers to the starting point of softening of the model material; $\alpha_1, \alpha_2, \alpha_3$ refer to the damage parameter variables of the model. This study applies modeling methods to characterize the rivet structure and conducts detailed simulations of the analytical units that make up the structure. By simulating the behavior of these units under load until failure, it is possible to predict the failure mode under specific loads and displacements, and help establish a deformation prediction model for rivet structures.

2.2. Design of riveting deformation prediction model

As riveting progresses, the rivets and connecting structural components will continuously accumulate nonlinear stress and strain. To predict riveting deformation, a separate local deformation analysis was conducted on riveting deformation. The necessity of conducting local deformation analysis alone lies in the fact that the stress-strain state in the local area during riveting may be extremely complex, with significant differences from non local areas. The local deformation data is first calculated using the finite element method, and then the overall deformation during the riveting process is predicted using an equivalent model. By combining local deformation data with equivalent models, it is possible to more accurately predict the overall deformation behavior of the entire riveted structure. In addition, the assumption of axisymmetric conditions originates from the symmetry of the connection geometry and loading conditions, which can significantly simplify the computational model, reducing the complexity and computational cost of the model. Therefore, this study assumes that the connector model has an axisymmetric condition, and the sum of the elongation of the rivet in the direction of the rivet joint is the overall elongation of the connector, as shown in Eq. (4) [18].

$$Y_L = n_p\left(2u_{r-p/2}\right) \tag{5}$$

In Eq. (5), Y_L refers to the overall elongation of the connecting unit; $u_{r-p/2}$ is the radial deformation of a single rivet at the position of half-rivet distance after riveting; n_p refers to the number of rivets on the model's single row of rivets. The radial elongation of countersunk head rivet is

shown in Eq. (6) [19].

$$u_{r-p/2} = \frac{(1+v)}{2Ep}(d_t)_2 K_r \left[\left(2\ln\frac{D_t}{D_0}\right)^{n_r} - \left(2\ln\frac{d_t}{D_0}\right)^{n_r}\right] \quad (6)$$

In Eq. (6), v refers to Poisson's ratio of rivet material; Ep is the elastic modulus of the material at the rivet distance; d_t indicates the average diameter of the riveted rod; K_r refers to the stress parameters of the rivet; D_t is the average diameter of the riveted pier head; D_0 is the diameter of the rivet; n_r is the radius of countersunk head. Ignoring the interaction between the connecting elements, the overall riveting warpage calculation process is shown in Eq. (7) [20].

$$Y_z = \frac{L + Y_{L2}}{Y_{L2} - Y_{L1}} h \sin^2 \frac{Y_{L2} - Y_{L1}}{h} \quad (7)$$

In Eq. (7), Y_z refers to the overall warping of the riveting; L refers to the initial length of the riveted structural part along the riveted joint; Y_{L1}, Y_{L2} represents the radial elongation of the skin skeleton; h denotes the total thickness of the laminated structure. The finite element analysis process of riveting in the assembly step is carried out in the modeling sequence of ABAQUS 2021 (Abaqus 6.9+VS2005+Intel Fortran 9.1/10.0/10.1) [21], and the specific process is as follows:

1. Solid model construction: Establish a solid model for riveting analysis in ABAQUS, defining material properties of each component, such as elastic modulus, Poisson's ratio, and density.

2. Definition of contact pairs: Based on the friction characteristics of the contact surface, simulate the physical connections between components.

3. Rivet insertion simulation: Select the contact surface between the rivet and the component to be riveted, and set the direction of rivet insertion.

4. Load and boundary condition settings: The simulation of riveting process and the limitation of component movement have a decisive impact [22, 23].

5. Solver parameter configuration: Adjust according to the complexity of the analysis problem and the required solution accuracy.

6. Result analysis: Obtaining data on stress, strain, and displacement after completing the analysis is crucial for understanding and optimizing the riveting process.

As shown in Fig. 3, this study establishes a cylindrical coordinate system, with each nail hole axis as the center, to measure the displacement and deformation before and after riveting. Multiple measurement points are selected equidistant on the axis, and a query tool is used to record the distance between the measurement points before and after riveting and the upper end face of the riveting die, to obtain the position information of the measurement points. Through this process, the position coordinates of the three rivets before and after deformation are captured [24]. It is observed that the interference of the nail hole significantly increases with the increase of the distance from the reference plane, leading to plastic deformation of the rivet head at the critical point. The corresponding nail hole axis also undergoes plastic deformation, bearing radial, axial, and tangential stresses. On this basis, further research is conducted to establish an elastic-plastic deformation model, which includes rules for local deformation fields to predict deformation behavior during batch riveting processes.

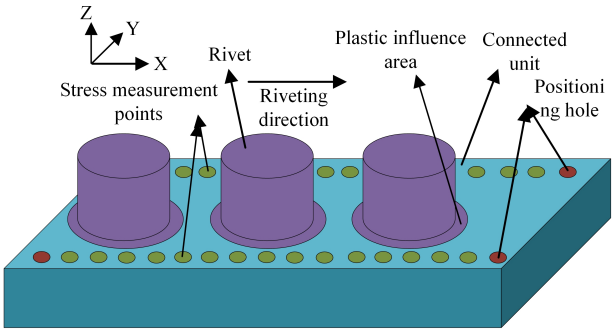

Fig. 3. Schematic diagram of rivet deformation and riveting sequence.

In Fig. 3, if the riveting model selects a datum plane, the deformation on the node object of the layer can be predicted by measuring the interference amount of the nail holes at different distances from the datum plane, which can be applied to the model of this study. In other words, the main plastic influence area of the model is divided into several layers along the direction of the connecting element, and the number of layers is determined by axial segmentation. In this way, the batch riveting model does not need to establish a model composed of rivets, connecting units, and upper and lower riveting molds one by one. In the finite element simulation case of single riveting deformation, the axial displacement and deformation of each layer of single riveting are recorded, and then these data are directly loaded into the model of batch riveting simulation laboratory as boundary conditions to achieve deformation prediction.

3. Performance test of riveted structure model and deformation prediction model

In this study, finite element simulation is conducted to investigate the deformation and stress distribution of riveted structures. ABAQUS 2021 software is used to establish U-shaped component models containing NAS1097KE5 and MS20470AD5 rivets. The simulation defines the contact surface as frictional contact and adjusts the material's elastic-plastic behavior through parameters' a 'and' b '. Select the nodes around the rivet holes as stress measurement points, and use a layered mapping algorithm to predict the displacement changes of U-shaped components under different loading angles. The load displacement relationship is presented through simulation of tensile experiments at different rates to characterize the structural performance of double nail lap riveting mode.

3.1. Riveting structure model test

The case setup used for measuring deformation/stress is ABAQUS 2021 (Abaqus 6.9+VS2005+Intel Fortran 9.1/10.0/10.1). This study selects two types of rivets, namely NAS1097KE5 and MS20470AD5. Among them, NAS1097KE5 is a 100 degree countersunk head rivet made of 7050-T73 aluminum alloy; MS20470AD5 is an oval head rivet made of 2117-T4 aluminum alloy. The material characteristics of rivets are shown in Table 1.

In this study, a group of U-shaped parts are designed for composite loading test. The bottom surface of two U-shaped parts "U" is connected by rivets, and both sides of "U" are connected with special test fixtures to complete the loading test of different angles of the riveted structure, including pure tensile, 30-degree composite loading, 45-degree composite loading, 60-degree composite loading, and pure shear. When modeling U-shaped riveted connections, the contact surface relationship is usually defined as frictional contact to simulate the interaction between riveted components. This contact algorithm needs to consider the positive pressure and friction characteristics between the contact surfaces. In this study, the test of 1.6mm+1.6mm U-shaped parts is simulated. A fully integrated Belytschko-Tsay shell element is adopted, and three integral points are set on the thickness [25], as shown in Fig. 4.

The mesh size of the finite element model is 2mm, with a total of 1974 nodes and 1832 shell elements. The boundary is set according to the case clamping condition, the lower end of the clamping section is constrained, and the upper end of the clamping section is loaded with velocity along the vector direction.

Fig. 5 shows the simulation results of U-shaped parts at different loading angles under four finite element analysis

Fig. 4. Riveting structure model of U-shaped parts.

elements. In the process of simulating the riveted structure of the beam element, the stress concentration occurs at the joint of the beam element and the U-shaped part, which is manifested as the structural failure of the joint element. For load tests from all angles, the solid unit can simulate the failure load very well. Fig. 5(a) shows the simulation results of the 8-hexahedral cluster and the 4-hexahedral cluster under pure tensile tests, with both configurations reaching maximum displacement at a load of 3500N. In the elastic stage, the simulation results are good, but in the plastic stage, the simulation results are high, and the simulation results of failure displacement are small, which shows that the model can simulate the elastic stage well under the condition of pure tension, but the accuracy of the simulation in the plastic stage and the failure stage needs to be improved. Fig. 5(b) shows the results of the 30° composite load simulation. It can be seen that with the decrease of the number of solid units, the simulation error of failure displacement gradually increases, which indicates that the number of solid units has a great influence on the simulation results under the combined load conditions. Fig. 5(c) shows the simulation results of a 60° composite load. Consistent with the results in Fig. 5(a), the model reaches its maximum displacement at a load of 3500N. Fig. 5(d) shows the simulation results under a pure shear test. Whether it is an 8-hexahedron cluster, a 4-

Table 1. Material Characteristics of Rivets.

Rivet model	Rivet type	Material	Rod diameter (mm)	Length (mm)
NAS1097 KE5	100 degree countersunk head rivet	7050 − T73 aluminum alloy	4.0	9.5
MS20470 AD5	Oval head rivet	2117 aluminum alloy	4.0	9.5

hexahedron cluster, or a hexahedron, the simulation results are basically the same, producing a maximum displacement value of 2mm under a load of about 4000N, which indicates that the model behaves consistently under pure shear conditions. The above data comparison results indicate that the 8-hexahedral cluster can more accurately predict the failure load and displacement under different loading conditions, especially in pure tensile tests, and its performance is better than other element types. Therefore, the 8-hexahedral cluster obtained the optimal results in finite element simulation. For this type of structure, using 8-hexahedral cluster for finite element modeling is the most appropriate.

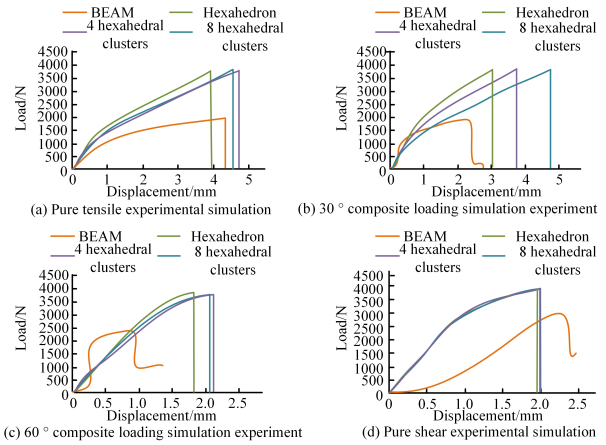

Fig. 5. Results of Composite Loading Simulation case.

In this study, parameters 'a' and 'b' are set to adjust the shape of the model during the elastoplastic phase. Parameters 'a' and 'b' are designed to more accurately simulate the deformation behavior of riveted structures. In particular, 'a' dominates the curve shape under pure tension and determines the performance of the model under tensile state, while 'b' mainly affects the curve shape under pure shear. Therefore, the setting of two parameters, 'a' and 'b', not only affects the shape of the model, but also determines the performance of the model, which plays an important role in understanding and solving the riveting deformation problem. Since the effects of both are similar, the study only tested the effects of 'a'. In the study, the value of a is changed to 1, 2, 4, 6 and 8 respectively, and then the pure tensile test is simulated. The change of load displacement curve is shown in Fig. 6. As the value of parameter a increases from 1 to 8, the simulated load displacement curve gradually moves upward, reflecting the enhanced energy absorption capacity of the model in the elastic-plastic stage. However, no matter how the value of a changes, the values of failure displacement and failure load remain unchanged, indicating that parameter a mainly affects the elastoplastic stage, but does not change the failure performance of the material.

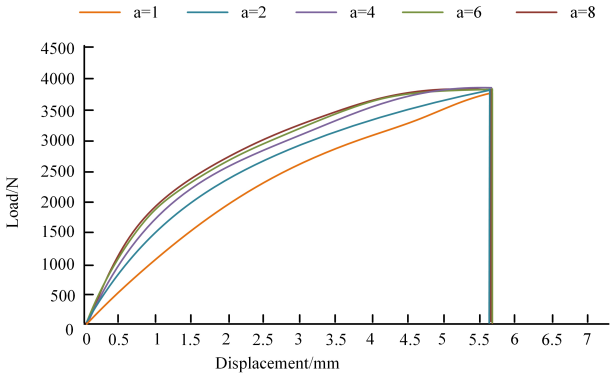

Fig. 6. Changes of load displacement under the influence of different a values.

The simulation case of the 60° composite loading model is carried out through damage parameter variables α_1, α_2 and α_3. α_1 and α_2 mainly affect the state of the load displacement curve before the failure of the model, which will increase the value of the failure load and failure displacement, while α_3 mainly affects the state of the load displacement curve during the damage stage of the model. The simulation case results are shown in Fig. 7. The load displacement curve did not produce large losses during the 60° composite loading case. In Fig. 7(b), α_2 has a significant effect on model failure, which is positively correlated with failure displacement and failure load, and the failure absorption capacity increases. The effect of α_1 and α_3 is small, and only when the value is larger, such as 8, will it have a significant impact. The simulation error of 8-clusters of hexahedral element and electrically connected constraint

element is compared to verify the performance of point-connected constraint element. The case results are shown in Table 1.

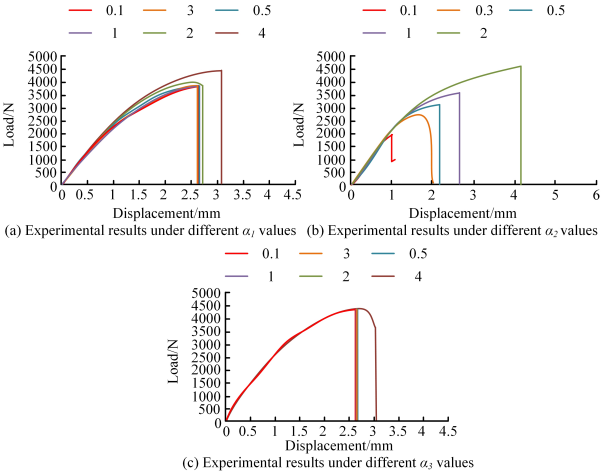

Fig. 7. Case results of load displacement under different loss parameters.

Table 2 shows the error data of 8-clusters of hexahedral element and point connection constraint element. The 8-clusters of hexahedral element is a riveting model based on the failure criterion of peak load, so the simulation error of failure load is minimal. The simulation errors of pure tensile and shear failure loads are 0.4% and less than 0.1% respectively, and the error of failure loads is less than 5%. However, the failure displacement error of 8-clusters of hexahedral element is large, the minimum error of pure shear failure displacement is 3.9%, the failure displacement error of 30° composite loading is 8.8%, and the failure displacement error of other angles is greater than 15%. Compared with 8-clusters of hexahedral element model, the error of failure load is slightly increased, but both are less than 10%. The point connection constraint model is a simplified riveting model, which abstracts the physical characteristics of the riveted structure and does not strictly follow the failure criterion of peak load. Therefore, the local stress concentration cannot be accurately simulated during the simulation of failure load, resulting in a slightly larger error in failure load compared with the 8-hexahedral cluster element model. The failure displacement error is only 14.6% under 30° compound loading, and less than 10% under other Angle compound loading. The overall simulation results of point connection constraint unit are good.

3.2. Test of rivet deformation prediction model

According to the layered mapping algorithm, the deformation prediction model is divided by interface function, and the finite element simulation case is carried out. The finite element analysis process module is consistent with the finite element analysis step of the common riveting model. Each node around the rivet holes in Fig. 3 is selected as a measuring point to study the stress distribution around the nail holes. The horizontal stitching holes numbered 1-8 are selected, and the horizontal stitching holes numbered 1-8 are selected to record the stress changes of the riveting holes during the riveting process. The selection of nodes around the rivet hole as stress measurement points is to accurately capture the contact stress distribution between the rivet and the hole wall during the riveting process. By measuring the points of horizontal stitching holes numbered 1-8, the stress concentration at the edge of the hole during rivet loading can be quantitatively analyzed, thereby evaluating the structural integrity and potential fatigue life of the riveted joint. Finally, the change of stress interaction between holes and nails in the riveting process is obtained. The test results are shown in Table 3.

As can be seen from the stress test results of the measuring points in Table 3, except for the stress of measuring point 1 at the No.1 nail hole, which is 487.1 MPa, the stress of other measuring points is lower than 20 MPa. Similarly, the stress at the measuring point of No. 1-8 nail hole is related to the nearest nail hole, and the longer the distance from the nail hole, the smaller the stress and the smaller the deformation effect on the rivet. Therefore, the influence of the remote measuring point on the nail hole is almost negligible, and the average stress on the connecting unit can be calculated to be 490 MPa. Five equidistant points on the far right of the connecting element of the rivet model are selected as measuring points to explore the horizontal and vertical deformation of the connecting element during the riveting process, as shown in Fig. 8.

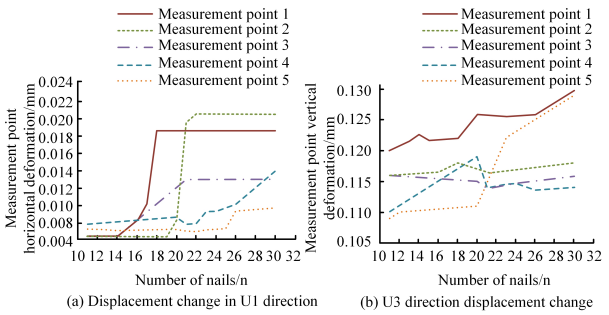

Fig. 8. Displacement changes during riveting.

Fig. 8 shows the displacement changes of "U1" and "U3" during the riveting process. Among them, "U1" represents the direction close to the riveting point, and "U3" represents the side direction located at the riveting point. In

Table 2. Simulation errors of the two models.

Model	8-clusters of hexahedral element		Point connection constraint unit	
Error	Failure displacement error (%)	Failure load error (%)	Failure displacement error (%)	Failure load error (%)
Pure drawing	17.6	0.4	7.7	0.9
30° Recombination	8.8	3.6	14.6	8.2
60° Recombination	27.2	1.5	5.8	5.4
Pure shear	3.9	0.0	9.6	2.9

Table 3. Simulation errors of the two models.

	Nail hole	1	2	3	4	5	6	7	8
Stress test results (S/MPa)	Measuring point 1	487.1	486.4	486.8	486.3	486.3	486.3	486.3	486.6
	Measuring point 2	15.0	499.7	487.1	486.3	486.2	486.6	485.2	485.5
	Measuring point 3	3.0	15.0	499.3	4866	486.5	486.7	486.7	486.7
	Measuring point 4	0.9	3.0	15.0	480.1	480.2	480.7	480.5	480.8
	Measuring point 5	0.9	2.0	2.0	483.4	487.6	486.1	487.1	486.5
	Measuring point 6	1.0	2.0	2.0	2.0	8.0	494.4	494.3	488.6
	Measuring point 7	1.0	2.0	2.0	2.0	2.0	8.4	485.9	486.1
	Measuring point 8	1.0	1.0	2.0	1.0	1.0	2.3	8.4	494.1

Fig. 8(a), the displacement trend of each stress measuring point in the horizontal direction is basically linear. Due to the micro-deformation of the single riveting, the change amount continuously accumulates along the skeleton direction, and the distance and constraint degree between different stress measuring points and nail holes are different, so the displacement change trend is inconsistent. In Fig. 8(b), with the progress of the riveting process, the deformation of stress measuring points 1, 3, 4 and 5 in the vertical direction increases significantly, and it can be inferred that these measuring points have gradually moved away from the riveting direction and the riveting point. When 21 rivet holes are riveted, the displacement of measuring point 2 in the vertical direction changes. The reason is that measuring point 2 is relatively close to the rivet hole, which can balance the warping deformation generated by several measuring points other than measuring point 2. However, after 21 rivet holes, the displacement of measuring point 1 and measuring point 5 in the vertical direction continues to increase during the riveting process, indicating that the displacement changes at different measuring points are different, the connection unit is unbalanced, and the riveting model will have continuous warping and concave deformation. The difference of the displacement trend in U1 and U3 is due to the difference of the position of the stress measuring point relative to the riveting point and direction. The linear increase of horizontal displacement is caused by the micro-deformation of single riveting. The vertical displacement increases significantly at measuring points away from the riveting direction and points, which are susceptible to warping and sag deformation.

In Fig. 9, EXP1, EXP2 and EXP3 represent case configurations with tensile speeds of 0.01m/s, 0.1m/s and 1 m/s, respectively. The selection of 0.01m/s, 0.1m/s, and 1m/s as tensile speeds is mainly based on industry standard testing rates, which can be considered as representative of low-speed and medium speed loading conditions encountered in practical applications. The hole edge distance of the riveted structure is only more than 2 times the diameter of the rivet, and the processing error of 1mm is allowed. The hole margin is 2 d+1 mm (d is the diameter of the rivet). The cross-riveting test of double nails is designed, and the diameter of retained nails is 4mm. The nail eye distance from the edge is 9mm; The connecting plate has a width of 28mm; The thickness of the attached substrate is 1.27mm. In the double riveted transverse riveting structure, there are two ways of damage: one is that a nail is cut, so that the connecting structure loses power, and the connecting plate is lifted; The other is to tear the splint between the two nail eyes, and turn the splint upward. Fig. 9 shows the variation of load-displacement in the three configurations. Through the average test of the three test points, the damage displacement and destructive power of the double-pin horizontal test point are 3.78mm and 6599N, respectively.

The SPR2 constraint model is a two-dimensional spring element applied in ABAQUS software, specifically designed to simulate contact and connection problems. This model defines in-plane rotation constraints through shear stiffness and torsional stiffness parameters, which can simulate relative rotation and displacement between materials, accurately reflecting the mechanical behavior of complex connections with high computational efficiency [26]. Then,

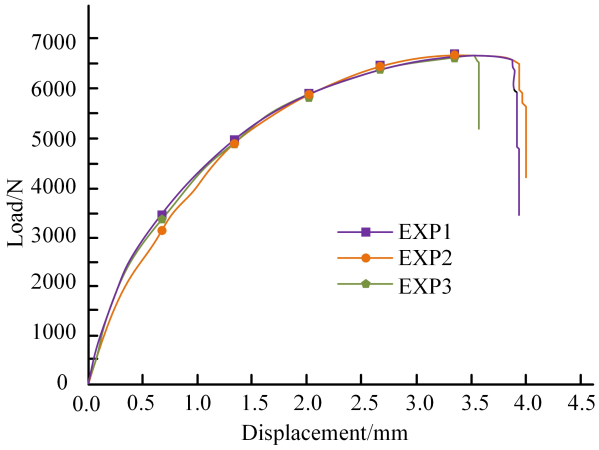

Fig. 9. Changes in load displacement under three configurations.

in this case, 8 hexagonal mass and SPR2 model are used to numerically simulate the double nail lap joint, and the load-displacement curves of the two nails are obtained, as shown in Fig. 10. 8 Hexagonal block riveting mode is to convert the damage degree of the connecting plate into nails, and the nails bear the main deformation.

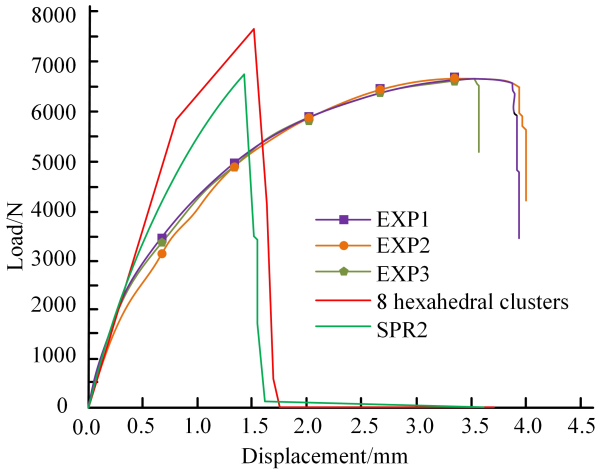

Fig. 10. 8-clusters of hexahedral and SPR2.

The hexagonal cluster riveting model was analyzed using ABAQUS in April 2023, and the simulation results revealed that rivets instead of connecting plates became the driving force for failure, confirming the importance of structural design. The SPR2 model accurately predicts the failure load, but there are still shortcomings in simulating displacement. The physical simulation uses an "I" type double rivet connection plate to display the stress distribution and failure mode of the connection plate, and the results are consistent with experimental data, verifying the reliability of the model. The 8-hexagon cluster riveting model translates the damage degree of the connecting plate into the rivet bearing the main deformation, so the final failure mode is the rivet failure as shown in Fig. 11(a), rather than the failure of the connecting plate. The resulting failure load is too high and the failure displacement is too low. SPR2 model can simulate failure load well, but it cannot simulate failure displacement well. The final simulation result shows that there is a shell element failure near the connection node, that is, at the set nail hole, as shown in Fig. 11(b). The final simulation results of the failure mode of a cylinder with holes are shown in Fig. 11(c). In Fig. 11(c), the cylinder is sliding directly out of the nail hole, and does not truly simulate the pressure of the connecting plate and the rivet. In Fig. 11(d), the "I" shape has holes in the solid simulation of the double-rivet connection plate, which is designed to accurately reproduce the interaction and failure mode between the rivet and the connection plate. This model can reflect the stress distribution of the connecting plate between rivets and simulate the structural failure caused by the failure of the connecting plate, which is consistent with the case results. Its advantage is that it can obtain accurate results in the simulation of failure load and displacement, which is of great value for understanding and optimizing the design of riveted structures. Fig. 11(d) shows the final simulation results of the physical destruction pattern of the "work" font with holes. In accordance with the case results, it is the failure of the connection structure caused by the failure of the connecting plate between the double nails. The simulation results that the method has achieved good results in the aspects of failure load and failure displacement.

4. Discussion

The case results show that the 8-hexahedral cluster model predicts accurately under different loads, especially in pure tension, which is consistent with the high accuracy of multi-element clusters in mechanical response simulation. The research results of this phenomenon in existing literature are consistent, and it is generally believed that multi-element clusters can provide more accurate mechanical response simulations. The model simulates accurately in the elastic stage, while the accuracy in the plastic and failure stages decreases. Further calibration of the material constitutive relationship and failure criteria is needed. As parameter a increases, the load displacement curve shifts upwards, indicating an increase in energy absorption capacity as deformation increases, but it does not affect the failure performance. Compared with the 8-hexahedral cluster, the point connection model has errors in predicting failure loads, but

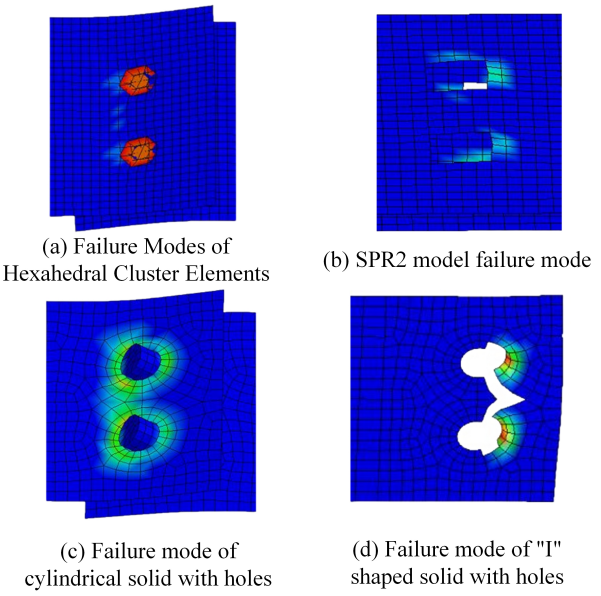

Fig. 11. Four Failure Modes.

the prediction of failure displacement is relatively accurate. By analyzing the performance of the 8-hexahedral cluster model under multi axis composite loads, it is observed that when a load at a different angle from the pure tensile test is applied, the predicted fault displacement of the model remains within 10% of the experimental data. This result demonstrates the robustness and reliability of the model under different loading conditions. The stress test shows that the stress changes significantly with the position of the nail hole, supporting the understanding of riveting deformation. The comparison between simulation and physical failure modes indicates that both rivet and connecting plate failures are important, emphasizing the need to comprehensively consider materials and connections when simulating complex structures. The displacement trend of each stress measurement point shows a specific pattern, which provides experimental basis for understanding the deformation behavior during riveting process and is supported by theoretical models in existing literature.

5. Conclusion

To analyze the riveted structure and establish the deformation prediction model, the finite element analysis method is used to model the riveted structure through small units, and the failure analysis of the riveted structure is carried out according to the multi-angle rivet load displacement case. Meanwhile, after the local element analysis, the layered mapping equivalent model is used to predict the deformation of the rivet structure, and the effect of the prediction model is verified by finite element simulation. The experimental results are as follows:

1. The point connection constraint model shows an error rate of no more than 10% in predicting failure loads, while under a 30° composite load, its failure displacement error is controlled at 14.6

2. Under the action of composite loads at different angles, the prediction error of the failure displacement of the model remains within 10%, indicating stable overall simulation performance of the model.

3. The prediction model reveals a negative correlation between the stress at the test point and the distance from the rivet hole. As the distance increases, the stress decreases, reaching a minimum of 0.9 MPa.

4. The deformation prediction model for riveted structures established through finite element analysis has been verified through multi angle load displacement experiments, and has been proven to have high accuracy and reliability in engineering applications.

5. The strong correlation between stress and rivet hole distance provides a basis for real-time monitoring of riveting structure deformation, which is helpful for deformation prediction and control in engineering.

The limitation of this study is that it failed to conduct dynamic analysis and verification, and future research directions can start from here.

References

[1] D. Liu, H. Chai, Z. Huang, Z. Guo, and Y. Bai, (2021) *"Multi-Field Model of Dual-Coil Electromagnetic Riveting and Riveted Streamline Feature with Annealed 7075 Aluminum Alloy"* **Journal of Materials Engineering and Performance *30***: 5568–5577. DOI: 10.1007/s11665-021-05831-z.

[2] A. Mohabeddine, J. Correia, J. Castro, P. Montenegro, A. De Jesus, and R. Calçada, (2021) *"Numerical investigation on the fatigue life of non-cracked metallic plates repaired with bonded CFRP"* **ce/papers *4***: 1135–1144. DOI: 10.1002/cepa.1405.

[3] T. Zhao, S. Li, Y. Wang, H. Wang, M. Zhang, X. Tang, F. Liu, D. Du, H. Zheng, and Y. Ma, (2021) *"Riveting the atomically distributed lithiophilic centers in the CNT-reinforced interfacial layer: an ultrathin, light-weight deposition substrate toward superior Li utilization"* **Journal of Materials Chemistry A *37***: 21281–21290. DOI: 10.1039/D1TA04741H.

[4] J. F. Valera-Jiménez, G. Burgueño-Barris, S. Gómez-González, J. López-López, E. Valmaseda-Castellón, and E. Fernández-Aguado, (2020) *"Finite element analysis of narrow dental implants"* **Dental materials *36***: 927–935. DOI: 10.1016/j.dental.2020.04.013.

[5] C. Ma, R. Scheichl, and T. Dodwell, (2022) *"Novel design and analysis of generalized finite element methods based on locally optimal spectral approximations"* **SIAM Journal on Numerical Analysis *60***: 244–273. DOI: 10.1016/j.apenergy.2021.117766.

[6] H. Bolandi, X. Li, T. Salem, V. N. Boddeti, and N. Lajnef, (2022) *"Bridging finite element and deep learning: High-resolution stress distribution prediction in structural components"* **SIAM Journal on Numerical Analysis *16***: 1365–1377. DOI: 10.1007/s11709-022-0882-5.

[7] J. A. N. Figueira and L. G. Trabasso, (2022) *"Riveting Squeezing Force Estimation: A Revised Algebraic Model"* **Journal of Aircraft *59***: 1005–1019. DOI: 10.2514/1.C036635.

[8] C. V. Zanatta, E. Villani, J. M. G. de Mello, and J. A. N. Figueira, (2022) *"Riveting process simulation to predict induced deformations in aeronautical structures"* **The International Journal of Advanced Manufacturing Technology *120***: 7673–7687. DOI: 10.1007/s00170-022-09247-4.

[9] P. Zamani and K. Farhangdoost, (2020) *"On the Influence of riveting process parameters on fatigue life of riveted lap joint"* **Journal of applied and computational mechanics *6***: 248–258. DOI: 10.22055/JACM.2019.28827.1507.

[10] S. Ji, X. Cui, L. Ma, H. Liu, Y. Zuo, and Z. Zhang, (2023) *"Achieving high-quality aluminum to copper dissimilar metals joint via friction stir double-riveting welding"* **Acta Metallurgica Sinica (English Letters) *36***: 552–572. DOI: 10.1007/s40195-022-01512-5.

[11] J. Wu and C. Chen, (2022) *"Experimental investigation of high impact polystyrene/metal self-piercing riveted joint"* **Polymers for Advanced Technologies *33***: 2221–2230. DOI: 10.1002/pat.5673.

[12] C. Song, B. Xing, X. He, and S. Wang, (2021) *"Self-piercing riveting for single-strap butt joints in similar aluminium alloys"* **Science and Technology of Welding and Joining *26***: 301–308. DOI: 10.1080/13621718.2021.19059.

[13] A. Mohamad, Z. Qasim, Q. Zhaoye, S. Babak, and A. Mohammed, (2020) *"Finite element analysis of natural fibers composites: A review"* **Nanotechnology Reviews *9***: 853–875. DOI: 10.1515/ntrev-2020-0069.

[14] N. Kardani, A. Zhou, M. Nazem, and S.-L. Shen, (2021) *"Improved prediction of slope stability using a hybrid stacking ensemble method based on finite element analysis and field data"* **Journal of Rock Mechanics and Geotechnical Engineering *13***: 188–201. DOI: 10.1016/j.jrmge.2020.05.011.

[15] H. Chen, D. Fan, J. Huang, W. Huang, G. Zhang, and L. Huang, (2020) *"Finite element analysis model on ultrasonic phased array technique for material defect time of flight diffraction detection"* **Science of Advanced Materials *12***: 665–675. DOI: 10.1166/sam.2020.3689.

[16] H. M. Numanoğlu, H. Ersoy, B. Akgöz, and Ö. Civalek, (2022) *"A new eigenvalue problem solver for thermo-mechanical vibration of Timoshenko nanobeams by an innovative nonlocal finite element method"* **Mathematical Methods in the Applied Sciences *45***: 2592–2614. DOI: 10.1002/mma.7942.

[17] A. B. Andhumoudine, X. Nie, Q. Zhou, J. Yu, O. I. Kane, L. Jin, and R. R. Djaroun, (2021) *"Investigation of coal elastic properties based on digital core technology and finite element method"* **Advances in Geo-Energy Research *5***: 53–63. DOI: 10.46690/ager.2021.01.06.

[18] M. Alipour, M. A. Torabi, M. Sareban, H. Lashini, E. Sadeghi, A. Fazaeli, M. Habibi, and R. Hashemi, (2020) *"Finite element and caseal method for analyzing the effects of martensite morphologies on the formability of DP steels"* **Mechanics Based Design of Structures and Machines *48***: 525–541. DOI: 10.1080/15397734.2019.1633343.

[19] K. Diao, X. Sun, G. Lei, Y. Guo, and J. Zhu, (2020) *"Multiobjective system level optimization method for switched reluctance motor drive systems using finite-element model"* **IEEE Transactions on Industrial Electronics *67***: 10055–10064. DOI: 10.1109/TIE.2019.2962483.

[20] Z. Zhang and C. Sun, (2021) *"Structural damage identification via physics-guided machine learning: a methodology integrating pattern recognition with finite element model updating"* **Structural Health Monitoring *20***: 1675–1688. DOI: 10.1177/147592172092748.

[21] T. Shen, B. Zhao, C. Wang, Y. Xiao, Y. Han, G. Zhao, and J. Ke, (2020) *"Efficacy of different designs of mandibular expanders: A 3-dimensional finite element study"* **American Journal of Orthodontics and Dentofacial Orthopedics *157***: 641–650. DOI: 10.1016/j.ajodo.2019.05.019.

[22] P. Liu and J. Sun, (2022) *"A new simple method to conveniently measure the open porosity of porous metal foams with reticular structure"* **Multidiscipline modeling in materials and structures *18***: 277–290. DOI: 10.1108/MMMS-11-2021-0175.

[23] A. Cortona, G. Rossini, S. Parrini, A. Deregibus, and T. Castroflorio, (2020) *"Clear aligner orthodontic therapy of rotated mandibular round-shaped teeth: a finite element study"* **The Angle Orthodontist *90***: 247–254. DOI: 10.2319/020719-86.1.

[24] N. Acharya, (2021) *"Finite Element Analysis on the Hydrothermal Pattern of Radiative Natural Convective Nanofluid Flow Inside a Square Enclosure Having Nonuniform Heated Walls"* **Heat Transfer *51***: 323–354. DOI: 10.1002/htj.22309.

[25] M. Uyaner, M. Kara, Y. Kepir, and A. Gunoz, (2023) *"Virtual testing of laminated composites subjected to low-velocity impact"* **Iranian Journal of Science and Technology, Transactions of Mechanical Engineering *47***: 595–610. DOI: 10.1007/s40997-022-00527-8.

[26] L. H. Binh and T.-V. T. Duong, (2021) *"Load balancing routing under constraints of quality of transmission in mesh wireless network based on software defined networking"* **Journal of Communications and Networks *23***: 12–22. DOI: 10.23919/JCN.2021.000004.